Electrical Power and Energy Systems 154 (2023) 109466

Contents lists available at ScienceDirect

International Journal of Electrical Power and Energy Systems

journal homepage: www.elsevier.com/locate/ijepes

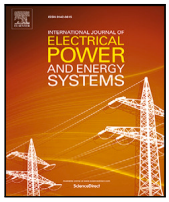

An impedance-multi-method-based fault location methodology for transmission lines connected to inverter-based resources

Moisés J.B.B. Davi [a,*], Mário Oleskovicz [a], Felipe V. Lopes [b]

[a] University of São Paulo (EESC-USP), São Carlos, 13566-590, São Paulo, Brazil
[b] Federal University of Paraíba (UFPB), João Pessoa, 58051-900, Paraíba, Brazil

ARTICLE INFO

Keywords:
Fault diagnosis
Fault location
Impedance-based fault location
Inverter-based generators
Multi-method

ABSTRACT

This paper is motivated by the growing penetration of Inverter-Based Resources (IBRs) in power systems and their impacts on fault diagnosis systems. Also, a motivating factor is the scarcity of works in the literature that evaluate the effects and provide solutions to impedance-based fault location in lines interconnecting IBRs to the grid. In this context, the performance of ten traditional impedance-based (one- and two-terminal) fault location methods is evaluated, and a multi-method methodology that minimizes the obtained fault location errors is proposed. To conduct the analysis and propose the methodology, the PSCAD software is used to carry out massive fault simulations on two systems with different voltage levels and connection topologies of IBRs to the grid. The results demonstrate that the proposed methodology significantly minimizes the fault location percentage errors, being a very promising proposal, especially for conditions in which communication channels between the line terminals are unavailable.

1. Introduction

In recent years, several researchers have focused on analyses of the Inverter-Based Resources (IBRs) fault contributions. It is due to the increasing penetration of these generators in the power system and their atypical operational characteristics that have impacted protection and fault diagnosis functions [1,2].

In this context, studies on the impacts of IBRs on the distance [3,4], directional [5,6], and phase-selection [6] protection functions have been widely disseminated in the literature. Furthermore, the proposition of new protection functions [7,8], as well as modifications in IBR controls [9,10] to favor the operation of traditional protection schemes have also been reported. However, there is a scarcity of studies that relate the problem of IBRs to fault diagnosis functions, such as impedance-based fault location methods, which will be the focus of this paper due to their importance and complexity.

Among the fault location methods available in the literature, those phasor-based that estimate the fault distance by monitoring the voltage and current signals from one or two line terminals stand out [11]. In the case of one-terminal methods, there are those based on the measurement of impedance [12], reactance [13], and Takagi methods [14] with their variations [11,15]. Among the two-terminal methods, Girgis [16], Johns and Jamali [17], Preston and Radojevic [18], and He [19] methods stand out. The problem is that with the emergence of IBRs and their atypical and control-dependent contributions [1,2], such approaches tend to present more expressive errors. However, an analysis of their performance for impedance-based fault location in lines interconnecting IBRs to the grid is still scarce in the literature.

When conducting a literature review of works assessing the impacts of IBRs on impedance-based fault location methods, there are papers with a greater focus on distribution systems [20,21]. In [20], a strategy for correcting the IBRs fault currents using energy storage systems is proposed, aiming to identify the faulty sections in the distribution system. In [21] a method based on two-terminal measurements is presented for fault location in inverter-dominated islanded microgrids. As one can see, the approaches treated are not directly applicable to transmission systems, and the impacts of IBRs on the aforementioned traditional fault location methods are not explored.

Moreover, in recent works such as [22,23] fault location methodologies are proposed for three-terminal lines considering the influence of renewable generations. However, besides not studying the impacts of IBRs on traditional fault location methods, the proposed methods rely on measurements from two or more terminals, and the influence of different IBR controls on the methods' performance is not evaluated.

Based on the presented context and recognizing the need for studies on this topic, the main contributions of this paper are:

- Quantification of IBR impacts on ten traditional impedance-based fault location methods;

* Corresponding author.
E-mail address: moisesdavi@usp.br (M.J.B.B. Davi).

https://doi.org/10.1016/j.ijepes.2023.109466
Received 6 March 2023; Received in revised form 3 July 2023; Accepted 24 August 2023
Available online 5 September 2023

- A proposal for modification of the zero-sequence Takagi method is presented, based on concepts initially proposed to improve distance protection [24], aiming to reduce the fault location errors for two-phase-to-ground faults;
- Based on the performance analyses of the mentioned fault location methods, a multi-method methodology [25] is proposed for fault location in lines interconnecting IBRs to the grid, aiming to minimize the errors obtained with the conventional methods.

This study considers two systems with different voltage levels and connection topologies of IBRs to the grid, modeled in the PSCAD software. The simulated fault situations on the lines connecting the IBRs assumed variations in several system parameters to obtain representative simulations.

2. Evaluated one-terminal methods

In this section, the evaluated one-terminal fault location methods are briefly described. Approaches not requiring knowledge of source impedances were prioritized since in the case of IBRs, the characteristics of these impedances are less predictable than those of conventional generations [26].

2.1. Impedance-based method (IMPE)

This method is based on fault distance estimation by calculating the section's positive sequence impedance between the measuring and fault points [12]. The estimated fault location (d), in p.u., is given by:

$$d = Re\left[\frac{\overrightarrow{V_r}/\overrightarrow{I_r}}{Z_{L1}}\right], \tag{1}$$

where $\overrightarrow{V_r}$ and $\overrightarrow{I_r}$ are the loop quantities, defined in Table 1, and Z_{L1} is the positive sequence impedance of the Transmission Line (TL). In Table 1, the subscripts *ra*, *rb*, and *rc* represent the quantities measured in phases A, B, and C, $K0$ is the zero sequence compensation factor, and $\overrightarrow{I_0}$ is the zero sequence current.

2.2. Reactance-based method (REAT)

This algorithm was proposed by [13], and its operation is very similar to the impedance-based method. However, aiming to reduce the influence of the fault resistances in fault location, this technique considers only the reactive portion of the estimated impedances, as shown in:

$$d = \frac{Im[\frac{\overrightarrow{V_r}}{\overrightarrow{I_r}}]}{Im[Z_{L1}]}. \tag{2}$$

It is worth noting that factors such as the system non-homogeneity and the capacitive effect of the TL still influence the results obtained with this algorithm.

2.3. Takagi methods (TAKS, TAKN e TAKZ)

The Simple Takagi Method (TAKS), uses incremental currents to reduce the effects of fault resistance and system loading [14]. The estimated location, in p.u., is defined by:

$$d = \frac{Im[\overrightarrow{V_r}\Delta\overrightarrow{I_r^*}]}{Im[Z_{L1}\overrightarrow{I_r}\Delta\overrightarrow{I_r^*}]}, \tag{3}$$

where $\Delta\overrightarrow{I_r}$ is the incremental current, determined by subtracting the fault samples from the pre-fault samples [14].

Based on the operational principle of the TAKS method, two others have emerged that, instead of using the incremental currents ($\Delta\overrightarrow{I_r}$), use the negative ($\overrightarrow{I_2}$) and zero ($\overrightarrow{3I_0}$) sequence components. Thus, these methods are known as Zero Sequence Takagi (TAKZ) and Negative Sequence Takagi (TAKN).

Table 1
Fault loop descriptions.

Fault loop	$\overrightarrow{V_r}$	$\overrightarrow{I_r}$
AG	$\overrightarrow{V_{ra}}$	$\overrightarrow{I_{ra}} + K0\overrightarrow{I_0}$
BG	$\overrightarrow{V_{rb}}$	$\overrightarrow{I_{rb}} + K0\overrightarrow{I_0}$
CG	$\overrightarrow{V_{rc}}$	$\overrightarrow{I_{rc}} + K0\overrightarrow{I_0}$
AB	$\overrightarrow{V_{ra}} - \overrightarrow{V_{rb}}$	$\overrightarrow{I_{ra}} - \overrightarrow{I_{rb}}$
BC	$\overrightarrow{V_{rb}} - \overrightarrow{V_{rc}}$	$\overrightarrow{I_{rb}} - \overrightarrow{I_{rc}}$
CA	$\overrightarrow{V_{rc}} - \overrightarrow{V_{ra}}$	$\overrightarrow{I_{rc}} - \overrightarrow{I_{ra}}$

3. Evaluated two-terminal methods

This topic describes the evaluated two-terminal methods, designed to reduce the influences of factors such as fault resistances on the localization task.

3.1. Girgis method (GG)

This method was proposed in [16] and uses the voltage at the fault point, calculated by measurements of both TL terminals to locate the fault distance (d) using:

$$\overrightarrow{V_{L_{abc}}} - \overrightarrow{V_{R_{abc}}} + l Z_{abc}\overrightarrow{I_{R_{abc}}} = d Z_{abc}(\overrightarrow{I_{L_{abc}}} + \overrightarrow{I_{R_{abc}}}), \tag{4}$$

where $V_{L_{abc}}$, $I_{L_{abc}}$, $V_{R_{abc}}$, and $I_{R_{abc}}$ are the voltages and currents at the local and remote TL terminals. Z_{abc} represents the TL series impedance matrix in the phase domain per unit length; l and d represent the total TL length and the fault distance, considering the local terminal as a reference.

3.2. Johns & Jamali method (JJ)

The method proposed in [17] considers the exact π model of the TL, contemplating the TL capacitive effects. The process estimates the fault point d, considering the local terminal as a reference, according to:

$$d = \frac{1}{\gamma l} tgh^{-1}\left[\frac{\overrightarrow{V_L} - \overrightarrow{V_R}\cosh(\gamma l) + \overrightarrow{I_R}Z_c\sinh(\gamma l)}{\overrightarrow{I_L}Z_c - \overrightarrow{V_R}\sinh(\gamma l) + \overrightarrow{I_R}Z_c\cosh(\gamma l)}\right], \tag{5}$$

where γ is the line propagation constant and Z_c is the TL characteristic impedance.

3.3. Preston & Radojevic method (PR)

This method, proposed in [18], considers the short-line model. The positive and negative sequence voltage and current phasors in both TL terminals are considered, and the fault location, in p.u., can be estimated from the expression:

$$d = \frac{\overrightarrow{\Delta V_{LR1}}\overrightarrow{I_{R2}} - \overrightarrow{\Delta V_{LR2}}\overrightarrow{I_{R1}}}{\overrightarrow{\Delta V_{LR1}}(\overrightarrow{I_{L1}} + \overrightarrow{I_{R2}}) - \overrightarrow{\Delta V_{LR2}}(\overrightarrow{I_{L1}} + \overrightarrow{I_{R1}})}, \tag{6}$$

where $\overrightarrow{\Delta V_{LR1}}$ and $\overrightarrow{\Delta V_{LR2}}$ represent the subtraction between the local and remote terminal positive and negative sequence voltages, respectively, $\overrightarrow{I_{L1}}$ represents the positive sequence currents at the local terminal, and $\overrightarrow{I_{L2}}$ and $\overrightarrow{I_{R2}}$ represent the negative sequence currents at local and remote terminals, respectively.

3.4. He method (HE)

This method considers the distributed parameters TL model and therefore the capacitive effects are considered [19]. Newton's iterative method is used to reduce the error in estimating the fault location. For the initial fault location estimation, the JJ method estimation is used. With this, the voltage at the fault point is estimated by the local ($\overrightarrow{V_{FL}}$) and remote ($\overrightarrow{V_{FR}}$) TL terminals (by (7) and (8)), and an objective function ($F_{dis}(d)$) dictated by the subtraction between these estimates

is created, as shown by (9). Finally, the derivative of the objective function is calculated and (10) is used for the iterative process.

$$\overrightarrow{V_{FL}} = \frac{\overrightarrow{V_{L1}} - \overrightarrow{I_{L1}}Z_c}{2} e^{\gamma(l-d)} + \frac{\overrightarrow{V_{L1}} + \overrightarrow{I_{L1}}Z_c}{2} e^{-\gamma(l-d)} \tag{7}$$

$$\overrightarrow{V_{FR}} = \frac{\overrightarrow{V_{R1}} - \overrightarrow{I_{R1}}Z_c}{2} e^{\gamma d} + \frac{\overrightarrow{V_{R1}} + \overrightarrow{I_{R1}}Z_c}{2} e^{-\gamma d} \tag{8}$$

$$F_{dis}(d) = \overrightarrow{V_{FL}} - \overrightarrow{V_{FR}} \tag{9}$$

$$d_{k+1} = d_k - \frac{F_{dis}(d_k)}{\frac{\partial F_{dis}(d_k)}{\partial d}} \tag{10}$$

When the difference between d_{k+1} and d_k is smaller than a threshold, d_{k+1} is assumed to be the fault location in p.u.

4. Performance analysis of evaluated methods

In this topic, performance analyses of the described methods are carried out to highlight in which scenarios each one is most effective. The percentage error is estimated using d_{ref} and d_{calc}, which are the reference and calculated distances, in p.u., respectively, by the equation $|d_{ref} - d_{calc}| \cdot 100$.

Boxplots are used to illustrate the results since it allows the survey of central quartiles (CQ), median, and outliers. In addition, the average error is also calculated and plotted on the charts. To provide better visualization of all evaluated methods' performance, the percentage error axis has been limited to 100% for one-terminal methods and to 25% for two-terminal approaches. The decision-making methods are considered with quantities measured 150 ms after the fault inception, waiting for the phasor stabilization, as well as the response time of the IBR controls [10].

Moreover, since the various factors related to IBRs that directly impact the decision-making of distance protection functions (such as the infeed effect, IBR modulation of negative sequence current, short-circuit currents with reduced levels, and others) have already been extensively discussed in the literature [3,4], and recognizing that such factors also tend to impact fault locators similarly, the analyses performed here will be solely aimed at surveying the percentage errors of each method evaluated, aiming to identify which methods perform better for certain fault conditions.

4.1. Test system for initial studies

For the initial studies in this paper, the test system whose single-line diagram and parameters are illustrated in Fig. 1 and Table 2, respectively, was employed. In this test system, the active and reactive powers supplied to the grid are controlled at 220.5 MW and 0 var, respectively. The wind power plant consists of 147 Full-Converter type Generators (FCG).

The modeling of FCGs for the studies in this paper is in line with the topologies already widely reported and consolidated in the literature [27,28]. The inverter controls were adjusted as described in [28]. The DC link consists of a 0.015 Farad capacitor with a nominal voltage of 1450 V. The coupling choke circuit has a resistance of 0.003 p.u. and an inductance of 0.15 p.u. at the machine base, and the RC output filter has a power of 120 kvar. The Chopper circuit was designed to operate when the DC link voltage exceeds 1.15 p.u. It is disabled when this voltage reaches values below 1.05 p.u. The nominal data for the permanent magnet synchronous generators are: Sn = 1.5 MVA; Vn = 690 V; Rs = 0.0017 p.u.; Xl = 0.0364 p.u.; Xd = 0.55 p.u.; Rkd = 0.055 p.u.; Xkd = 0.62 p.u.; Xq = 1.11 p.u.; Rkq = 0.183 p.u.; and Xkq = 1.175 p.u..

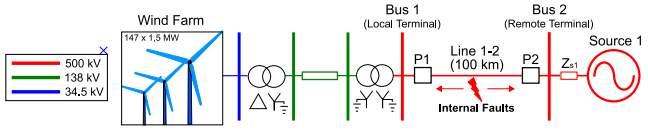

Fig. 1. Test system single-line diagram.

Table 2
Test system parameters.

Parameters	Values
Source 1	V_{s1} = 500 ∠ 0° kV R+/0 = 0.984/3.447 Ω L+/0 = 28.732/57.467 mH
Transformer Dyn11 (34.5 – 0.575 kV)	1.75 MVA - Z = 6%
Transformer YNd1 (138 – 34.5 kV)	90 MVA - Z = 10%
Transformer YNyn0 (500 – 138 kV)	250 MVA - Z = 10%
Line 1–2	R+/0 = 0.017/0.331 Ω/km L+/0 = 0.839/2.382 mH/km C+/0 = 0.0137/0.0082 μF/km

Table 3
Descriptions of the IBRs' considered controls.

Group	Characteristics
Group 1 Controls (G1C)	G1C represent the emerging strategies, whose operation is based only on positive sequence components (Coupled Sequence Controls [26]). This control suppresses the negative sequence currents, even for asymmetrical disturbances [29].
Group 2 Controls (G2C)	G2C inject additional levels of reactive current after the fault detection, which is dictated by the voltage variation measured at the IBR coupling point. In this strategy, negative sequence currents are also provided (Decoupled Sequence Control [26]) and injected with levels proportional to the negative sequence voltages [10].

Short circuits are simulated, varying: the type (AG, BG, CG, AB, BC, CA, ABG, BCG, CAG, and ABC); phase resistance (R_p equal to 0, 1, 1.5, and 2 Ω); ground resistance (R_g equal to 0, 25, 50, and 100 Ω); inception angle (0° and 90°); and fault location (from 0% to 100% of Line 1–2 with a step of 10%, being 0% the point P1).

The choice of smaller values for the fault resistances between phases (R_p) was based on the fact that this resistance is dictated by the electric arc formed between the phases, which presents low resistance values [30]. In contrast, the resistances (R_g) can reach higher values for phase-to-ground faults due to, for example, the contact of vegetation with the system phases (typical resistance values up to 100 ohms [31]). Thus, aiming to make the analysis more reliable in practical terms, such values for the variation of the fault resistances were chosen.

For the simulations, two IBRs' control types were considered, referred to in this paper as Group 1 Controls (G1C) and Group 2 Controls (G2C). The characteristics of these controls are described in Table 3. Moreover, the Source 1 short circuit level was changed using a Short Circuit Level Multiplier (SCLM) that represents how many times the Source 1 short circuit power is greater than the wind power plant rated power. This multiplier varied between 10, 25, 50, and 100. Considering variations in the IBRs' controls, grid short circuit level, and fault parameters, 28 160 scenarios were evaluated.

In all simulated scenarios, the current and voltage signals are obtained from the secondary windings of current and potential transformers, whose transformation ratios are 60 and 4500, respectively. These transformers are installed at point P1, illustrated in Fig. 1.

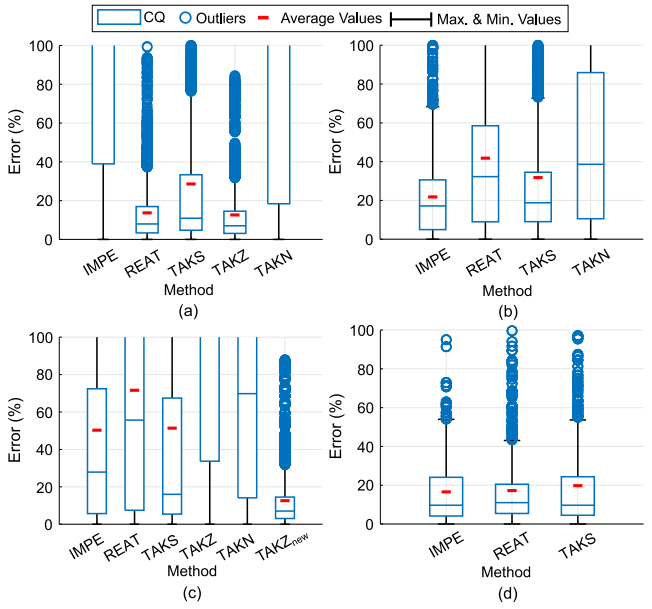

Fig. 2. Performance of one-terminal methods for (a) PG, (b) PP, (c) PPG, and (d) PPP fault types.

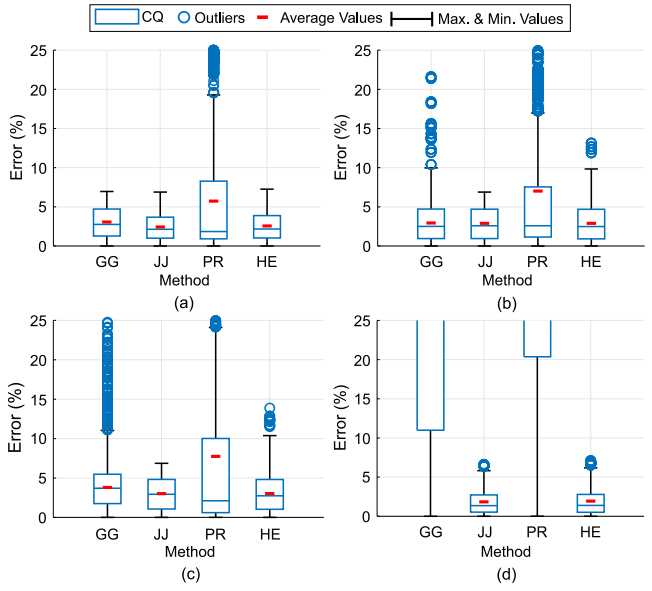

Fig. 3. Performance of two-terminal methods for (a) PG, (b) PP, (c) PPG, and (d) PPP fault types.

4.2. Preliminary performance analysis

At first, the fault location percentage errors, by fault type (Phase-to-Ground (PG), Phase-to-Phase (PP), Phase-to-Phase-to-Ground (PPG), and Three-Phase (PPP) faults), for all simulated scenarios are assessed. Figs. 2 and 3 illustrate the obtained errors for measurements at the local terminal, considering one-terminal and two-terminal methods, respectively.

This initial analysis aims to select at least two of the best-performing methods for each fault type. It is emphasized that the percentage errors for measurements at the remote terminal (see Fig. 1) were also evaluated. As expected, the errors obtained were quite small (less than 10%) because it is a terminal that measures conventional generation contributions for faults in Line 1-2 [25]. Therefore, the demonstrated results focus on measurements at point P1 (IBR side).

Table 4
New phase-to-phase fault loop descriptions.

Fault loop	$\overrightarrow{V_r}$	$\overrightarrow{I_r}$
AB_{new}	$\overrightarrow{V_{ra}} + \overrightarrow{V_{rb}}$	$\overrightarrow{I_{ra}} + \overrightarrow{I_{rb}} + 2K0\overrightarrow{I_0}$
BC_{new}	$\overrightarrow{V_{rb}} + \overrightarrow{V_{rc}}$	$\overrightarrow{I_{rb}} + \overrightarrow{I_{rc}} + 2K0\overrightarrow{I_0}$
CA_{new}	$\overrightarrow{V_{rc}} + \overrightarrow{V_{ra}}$	$\overrightarrow{I_{rc}} + \overrightarrow{I_{ra}} + 2K0\overrightarrow{I_0}$

When conducting some preliminary analyses, it was noticed that, for PPG faults, the obtained errors were very high for the traditional methods. Thus, in an attempt to reduce the errors observed for this fault type, the loop magnitudes shown in Table 4, initially proposed by [24] for improving distance protection, were used to modify the TAKZ method. Thus, the TAKZ method with this modification is also evaluated in this paper for PPG faults and is referred to as TAKZ$_{new}$.

Regarding the results for one-terminal methods, the main conclusions for each fault type are given below:

- For PG faults, the REAT and TAKZ methods stand out with average errors of 13.71% and 12.63%, respectively;
- Considering PP faults, the IMPE and TAKS methods were highlighted by the best performances, with mean errors of 21.81% and 31.79%, respectively;
- For PPG faults, the TAKZ$_{new}$ method was by far the best performer (average error of 12.59%), followed by the IMPE method with an average error of 50.27%;
- Finally, for PPP faults, it is observed that for the IMPE, REAT, and TAKS methods, similar average errors of 16.57%, 17.24%, and 19.78% were obtained, respectively.

Regarding the results for the two-terminal techniques, it can be seen that the JJ and HE methods presented the smallest errors regardless of the fault type. This is expected since both methods consider more complete models of the TLs, contemplating, for example, the lines' capacitive effect that directly influences impedance-based fault location methods.

4.3. Detailed analysis (one-terminal methods)

After the preliminary analysis and identification of the best-performing methods for each fault type, a more detailed performance study of the selected methods is carried out, using boxplots, considering filters for other system parameters (fault resistances, SCLM, and IBRs control groups). The detailed analyses aim, besides proving which is the best method among the selected ones in the preliminary investigation, to highlight new conditions that allow the reduction of the location error of the methodology to be proposed in this work.

Fig. 4 illustrates the performance of the REAT and TAKZ methods for PG faults. It is observed that the increment of R_g, as expected, increased the method's location errors since the fault resistance changes the impedance to be estimated. However, it can be concluded that the TAKZ method remains with better performance for all considered R_g filters. By increasing the value of SCLM, it is observed that the errors are also higher, i.e., grids with higher short circuit levels will result in a more pronounced remote infeed effect, characterized by the voltage drop in the fault resistance produced by the remote terminal fault contributions. This situation naturally impacts the impedance estimated by the local terminal methods (IBRs side). However, it is also noted that the TAKZ method holds up with better performance. Finally, when varying the IBRs control type, it is observed that the errors obtained for the TAKZ method are also minor.

Regarding the performance of IMPE and TAKS methods for PP faults, illustrated in Fig. 5, the obtained errors are also higher by increasing the R_p and SCLM values. However, in general, the IMPE method presents lower errors. Varying the IBRs control type, when considering the G1C, the TAKS method has a better performance. When

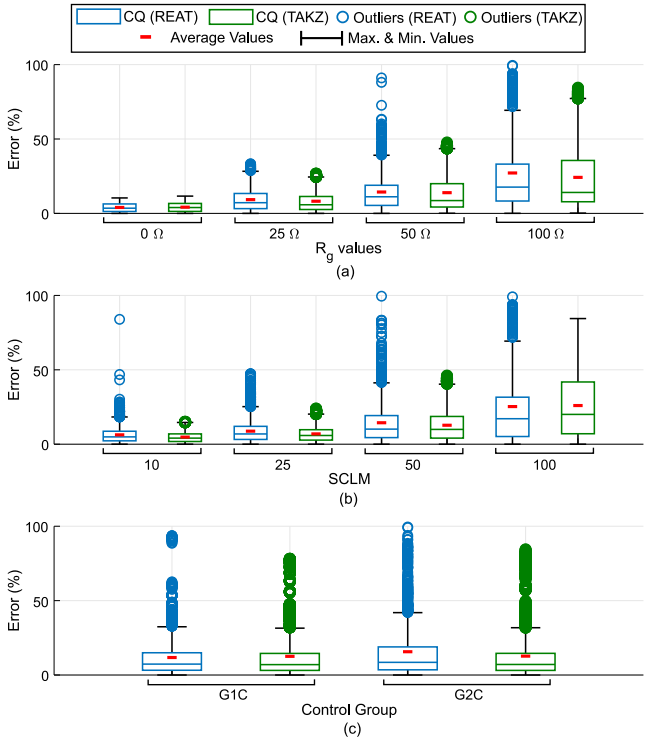

Fig. 4. Performance of the REAT and TAKZ methods for PG faults, varying (a) R_g values, (b) SCLM, and (c) control groups.

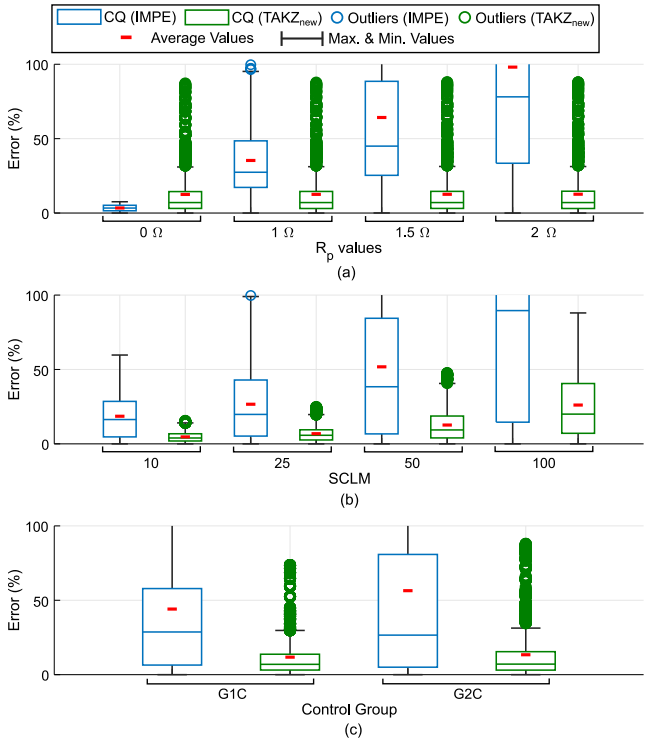

Fig. 6. Performance of the IMPE and TAKZ$_{new}$ methods for PPG faults, varying (a) R_p values, (b) SCLM, and (c) control groups.

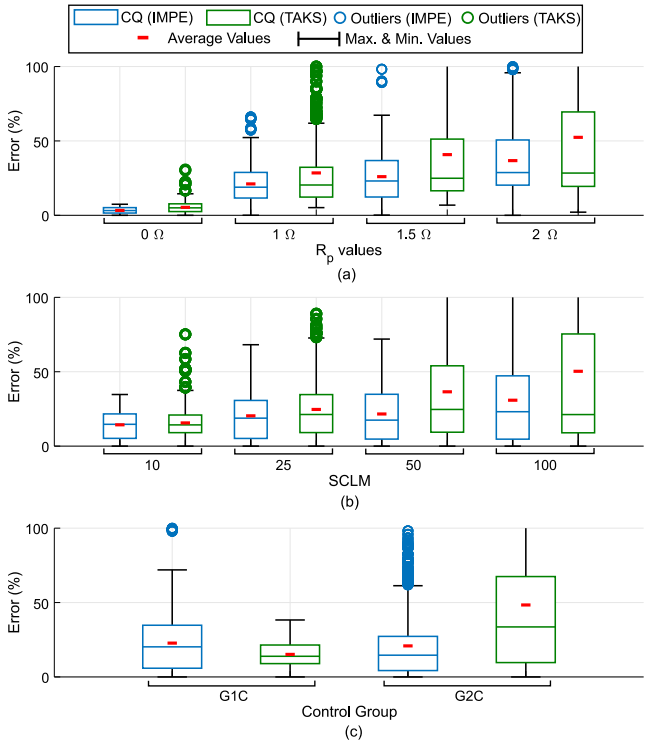

Fig. 5. Performance of the IMPE and TAKS methods for PP faults, varying (a) R_p values, (b) SCLM, and (c) control groups.

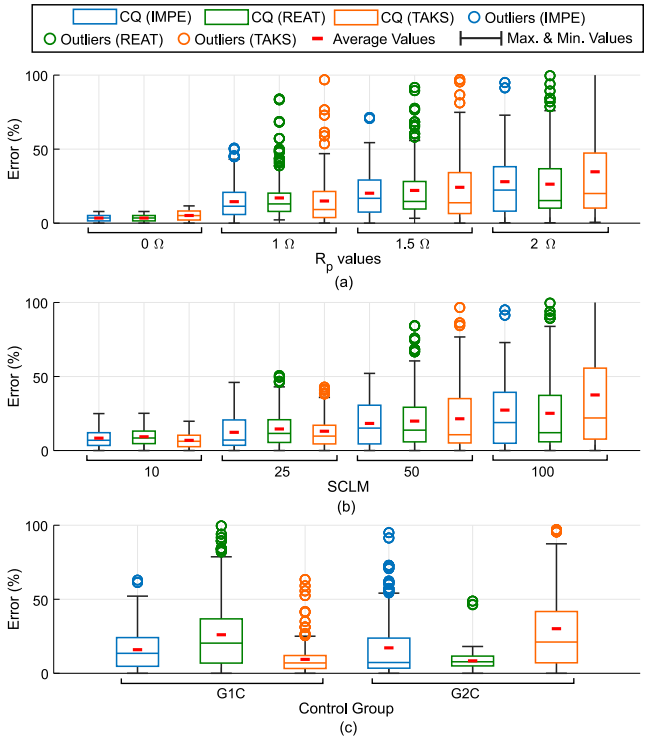

Fig. 7. Performance of the IMPE, REAT, and TAKS methods for PPP faults, varying (a) R_p values, (b) SCLM, and (c) control groups.

considering the G2C, the IMPE method is more effective. However, the obtained errors are similar between the two evaluated methods.

Moving on to the PPG fault analyses for the IMPE and TAKZ$_{new}$ methods, with performance illustrated in Fig. 6, it is observed that, except for the filtered scenarios for $R_p = 0\ \Omega$, the TAKZ$_{new}$ technique showed significantly lower location errors than those obtained for the IMPE method. It is also noted that the increase in localization errors with the increment in R_p and SCLM values is much more subtle for the

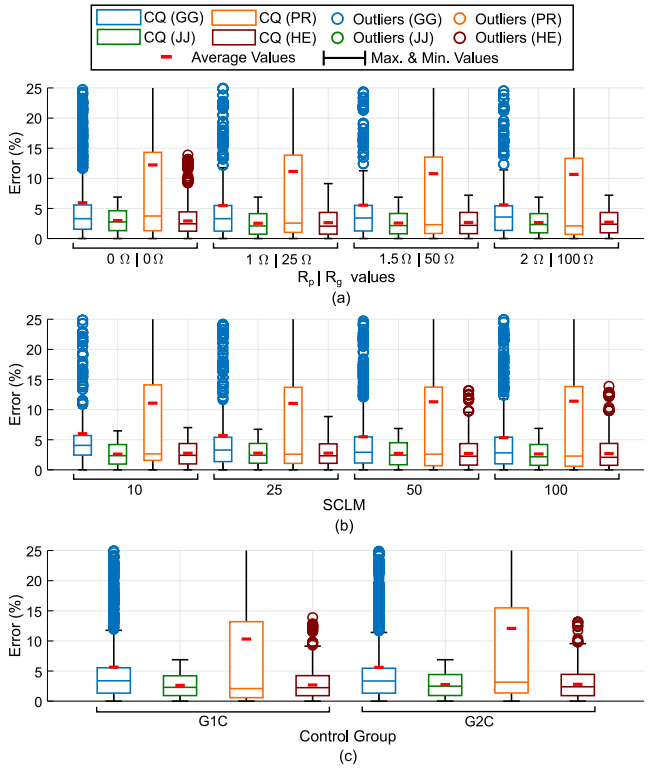

Fig. 8. Performance of the GG, JJ, PR, and HE methods for all fault types, varying (a) $R_p|R_g$ values, (b) SCLM, and (c) control groups.

TAKZ$_{new}$ method, which proves its superiority for localizing PPG faults in systems with IBRs.

Considering the performance of IMPE, REAT, and TAKS methods for PPP faults, illustrated in Fig. 7, it is noticed that the errors obtained with a variation of the parameters R_p and SCLM are similar for the three methods. However, when varying the IBRs control type, it is noted that considering the G1C, even with the existence of outliers, the TAKS method presents lower average errors. In contrast, considering the G2C, the REAT method showed superiority among the three pre-selected methods.

4.4. Detailed analysis (two-terminal methods)

Similar to the studies performed for the one-terminal methods, the two-terminal techniques were evaluated by considering filters for fault resistance, SCLM, and IBR control parameters. Fig. 8 illustrates the performance of the GG, JJ, PR, and HE methods for all fault types.

It is noted that regardless of the parameter filtered, the JJ method presents the lowest errors among the evaluated methods. Furthermore, it can be observed that this method keeps stable operation, with reduced errors, even with an increase in the fault resistance, an increase of the grid short circuit level, or a variation of the IBR control type.

4.5. Additional detailed analyses (one- and two-terminal methods)

As a complement to the detailed analyses previously performed, filters for the parameters of fault inception angle and fault location were also applied, considering the best-performing methods for each fault type. Figs. 9, 10, 11 and 12 illustrate the errors for PG, PP, PPG, and PPP faults, respectively, considering the one-terminal best-performing methods. Fig. 13, on the other hand, illustrates the errors for the two-terminal methods.

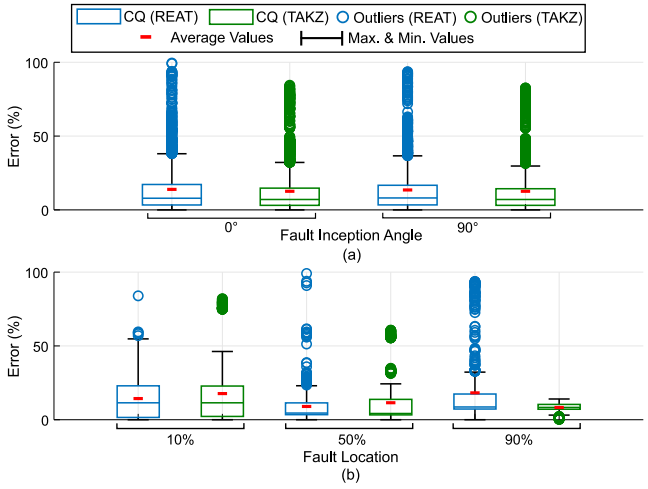

Fig. 9. Performance of the REAT and TAKZ methods for PG faults, varying (a) fault inception angle and (b) fault location.

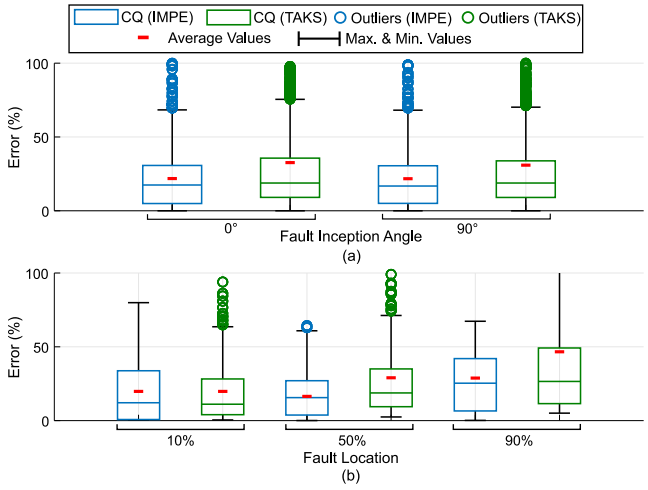

Fig. 10. Performance of the IMPE and TAKS methods for PP faults, varying (a) fault inception angle and (b) fault location.

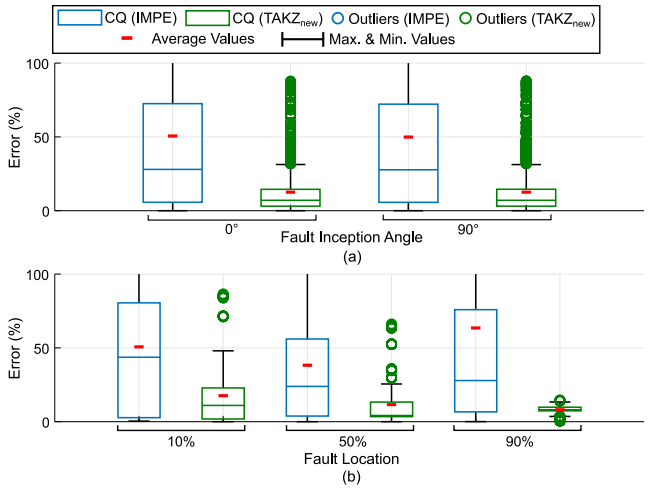

Fig. 11. Performance of the IMPE and TAKZ$_{new}$ methods for PPG faults, varying (a) fault inception angle and (b) fault location.

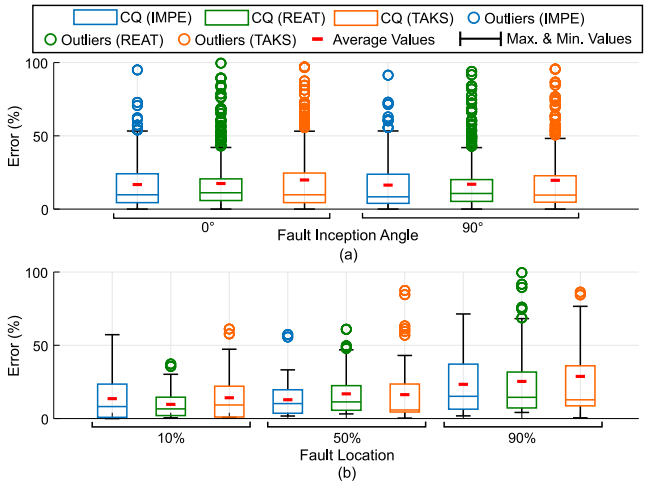

Fig. 12. Performance of the IMPE, REAT, and TAKS methods for PPP faults, varying (a) fault inception angle and (b) fault location.

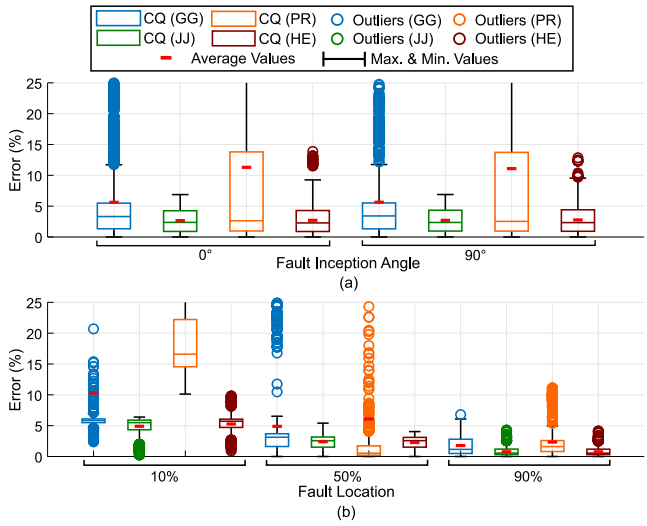

Fig. 13. Performance of the GG, JJ, PR, and HE methods for all fault types, varying (a) fault inception angle and (b) fault location.

Assessing the results, first considering the fault inception angle filter, the figures illustrate that varying this parameter had no significant influence on the obtained errors for the evaluated fault location methods.

Regarding the fault location filter, a more significant influence is observed for the TAKZ and TAKZ$_{new}$ methods, in PG and PPG fault scenarios. In these cases, as the fault is closer to the remote terminal (Bus 2), the obtained errors are reduced. This condition occurs because, in fault scenarios with ground involvement, the remote infeed effect is basically dictated by the zero-sequence current, which comes from the grid returning through the grounded neutral point of the Bus 1 transformer, and also by the remote terminal current contributions [24]. Since the remote terminal current contributions tend to increase as the fault approaches the remote terminal, the effect of the IBRs' positive sequence fault contributions on the remote infeed is decreased and, consequently, the errors obtained by the fault location methods are also reduced [24].

5. Proposed fault location methodology

After the preliminary and detailed analyses, it was possible to draw some conclusions:

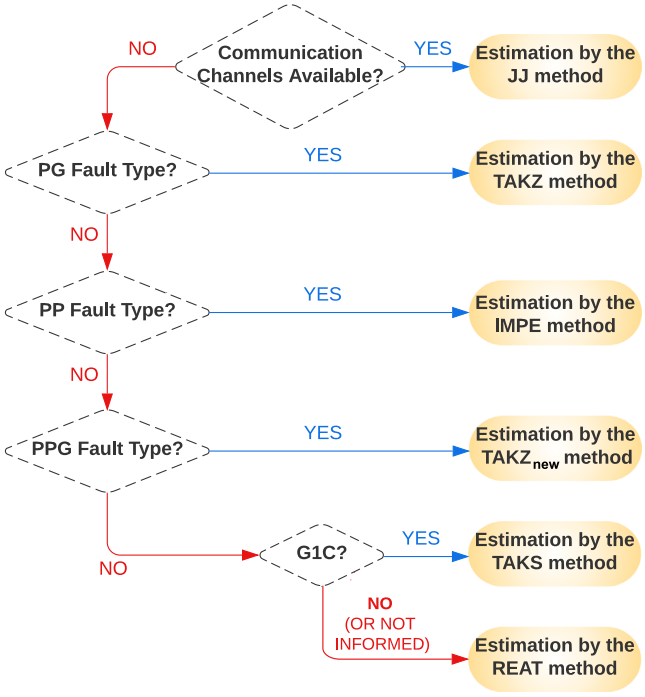

Fig. 14. Flowchart of the proposed impedance-multi-method-based fault location methodology.

- In case communication channels are available, the two-terminal methods should be used, emphasizing the JJ method, which presented the lowest errors among those evaluated. If the communication channels are not available, the fault type and the IBR control type should be considered, aiming to select the method with the slightest error, as will be discussed in the topics below;
- For PG faults, the TAKZ method showed the best performance among the one-terminal methods;
- Regarding PP faults, the IMPE method showed the best performance among the one-terminal methods;
- For PPG faults, it was observed that all the conventional methods presented very high errors, and the TAKZ$_{new}$ method was the most suitable for this fault type;
- Finally, for PPP faults, it is noted that for G1C the TAKS method performed best. For G2C the REAT method was favored, and finally, in general, if the IBR control type is unknown, the REAT method provided the lowest errors.

Considering all the observations mentioned above and that there is a previous fault classification module before, it was possible to propose an impedance-multi-method-based fault location methodology, shown in Fig. 14, which aims to minimize fault location errors for systems with IBRs, being the main contribution of this paper.

6. Quantitative performance analysis of the proposed methodology

The proposed methodology's effectiveness is proved by comparing its average percentage of errors per fault type with all other evaluated methods. To do so, the 28 160 fault scenarios simulated in the initial test system (Topic 4.1) were considered.

Tables 5, 6, and 7 show the average percentage errors for three different conditions, respectively: (1) It is considered that the communication channels are not available, and the user is aware of the IBR control type; (2) It is considered that the communication channels are not available, and the user is not aware of the IBR control type;

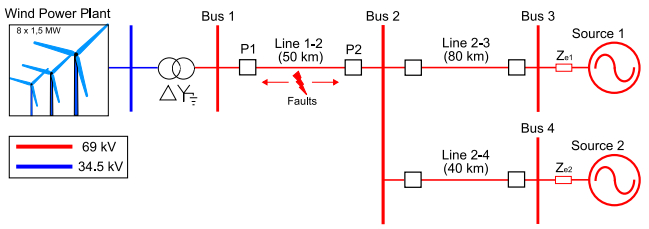

Fig. 15. Test system single-line diagram.

Table 5
Average percentage errors for Condition 1.

	IMPE	REAT	TAKS	TAKZ	TAKN	**Proposed**
PG	339%	13.7%	28.6%	12.6%	2241%	**12.6%**
PP	21.8%	41.8%	31.8%	–	111%	**21.8%**
PPG	50.3%	71.6%	51.4%	754%	505%	**12.6%**
PPP	16.6%	17.2%	19.8%	–	–	**8.9%**
All	**125%**	**39.8%**	**35.5%**	**383%**	**952%**	**15.0%**

Table 6
Average percentage errors for Condition 2.

	IMPE	REAT	TAKS	TAKZ	TAKN	**Proposed**
PG	339%	13.7%	28.6%	12.6%	2241%	**12.6%**
PP	21.8%	41.8%	31.8%	–	111%	**21.8%**
PPG	50.3%	71.6%	51.4%	754%	505%	**12.6%**
PPP	16.6%	17.2%	19.8%	–	–	**17.2%**
All	**125%**	**39.9%**	**35.5%**	**383%**	**952%**	**15.8%**

Table 7
Average percentage errors for Condition 3.

	GG	JJ	PR	HE	**Proposed**
PG	3.06%	2.43%	5.73%	2.56%	**2.44%**
PP	2.94%	2.89%	7.01%	2.89%	**2.89%**
PPG	3.81%	3.02%	7.73%	3.03%	**3.02%**
PPP	26.96%	1.84%	50.53%	1.94%	**1.85%**
All	**5.64%**	**2.69%**	**11.20%**	**2.74%**	**2.69%**

(3) It is considered that the communication channels are available. Naturally, the one-terminal methods were considered for the evaluation of conditions 1 and 2, and for condition 3, the two-terminal techniques were explored.

According to Table 5, the overall average error of the proposed methodology, considering all fault types, was 15%, which represents a reduction of 57.7% if compared to the TAKS method, which presented the best performance among traditional methods for this condition. Table 6 shows that not knowing the IBR control type (Condition 2) resulted in higher average error percentages for PPP faults, reflecting an overall error (for all fault types) of 15.8%, still with a significant reduction if compared to the TAKS method. Finally, Table 7 shows that the availability of communication channels results in significantly reduced errors, and the proposed approach, in this condition, is represented by the JJ method.

7. Testing other power system topologies: Validating the proposed methodology's generalizability

Aiming to explore the proposed methodology's generalizability to other power system structures, voltage levels, fault inception angles, and load flows, a second test system with a single-line diagram and parameters shown in Fig. 15 and Table 8, respectively, is considered.

This is a 69 kV sub-transmission system, with Bus 1 being the common coupling point between the wind power plant and the grid. The wind power plant consists of eight FCG of 1.5 MVA each, connected to the 34.5 kV system by Dyn11 transformers with voltages of 34.5–0.575 kV, powers of 1.75 MVA, and impedances of 6%. TLs of 50, 80, and 40 km connect buses 1–2, 2–3, and 2–4, respectively. At buses 3 and 4, Thevenin equivalent systems represent the grid.

Table 8
Test system parameters.

Parameters	Values
Source 1	V_{s1} = 71.76 ∠ 0° kV R+/0 = 0.112/0.435 Ω L+/0 = 16.976/48.805 mH
Source 2	V_{s2} = 70.38 ∠ −25° kV R+/0 = 0.431/1.678 Ω L+/0 = 65.507/188.330 mH
Transformer YNd1 69 – 34.5 kV	14 MVA - Z = 10%
Transmission lines	R+/0 = 0.159/0.516 Ω/km L+/0 = 1.327/3.929 mH/km C+/0 = 0.0087/0.0059 μF/km

Table 9
Average percentage errors for Condition 1.

	IMPE	REAT	TAKS	TAKZ	TAKN	**Proposed**
PG	146%	22.1%	29.7%	2.61%	1144%	**2.61%**
PP	12.5%	14.3%	118%	–	21.1%	**12.5%**
PPG	51.1%	35.5%	9899%	430%	134%	**3.09%**
PPP	7.49%	4.85%	11.1%	–	–	**6.41%**
All	**63.3%**	**22.1%**	**3015%**	**216%**	**433%**	**6.09%**

Table 10
Average percentage errors for Condition 2.

	IMPE	REAT	TAKS	TAKZ	TAKN	**Proposed**
PG	146%	22.1%	29.7%	2.61%	1144%	**2.61%**
PP	12.5%	14.3%	118%	–	21.1%	**12.5%**
PPG	51.1%	35.5%	9899%	430%	134%	**3.09%**
PPP	7.49%	4.85%	11.1%	–	–	**4.85%**
All	**63.3%**	**22.1%**	**3015%**	**216%**	**433%**	**5.93%**

Table 11
Average percentage errors for Condition 3.

	GG	JJ	PR	HE	**Proposed**
PG	0.10%	0.41%	1.32%	0.48%	**0.41%**
PP	0.08%	0.19%	1.64%	0.26%	**0.19%**
PPG	0.11%	0.15%	1.69%	0.16%	**0.15%**
PPP	7.37%	0.11%	29.3%	0.12%	**0.11%**
All	**0.82%**	**0.24%**	**4.33%**	**0.28%**	**0.24%**

The active and reactive powers supplied by the FCG were kept at 12 MW and 0 var, respectively. For the control of the FCG, G1C and G2C (see Table 3) were considered. Aiming to evaluate the impact of the grid short circuit level on the studies, the short circuit power of Sources 1 and 2 were set according to two different scenarios: (1) Source 1 (800 MVA) and Source 2 (200 MVA); (2) Source 1 (80 MVA) and Source 2 (20 MVA). The FCG controls were adjusted as described in [27,28].

Short circuits were simulated on Line 1–2, varying the type (AG, BG, BG, AB, BC, AC, ABG, BCG, CAG, and ABC), the resistance between phases (0, 1, 1.5 and 2 Ω), the resistance between phases and ground (0, 25, 50 and 100 Ω), the fault inception angle (0, 45 and 90 degrees), and fault distance (from 0% to 100% of Line 1–2 with a step of 10%, being 0% the point P1). Thus, considering variations in the sources' short circuit levels and different control groups, 21 120 additional scenarios were simulated and evaluated.

In all scenarios, the current and voltage signals were obtained from the secondary windings of current and voltage transformers, whose transformation ratios are 20 and 600, respectively. These instrument transformers were installed at point P1 illustrated in Fig. 15.

Tables 9, 10, and 11 show the average error percentage of the proposed methodology when compared to conventional methods, for the same three conditions presented in Tables 5, 6, and 7: (1) Commu-

nication channels not available, and the IBR's control type is known; (2) Communication channels not available, and the IBR's control type is not known; (3) Communication channels available.

Through the obtained results for the new test system, it can be concluded that the proposed methodology decreased by 73% the average error obtained by the best among the traditional fault location methods (REAT) for conditions 1 and 2 (one-terminal methods). Moreover, the proposed methodology remained the method that resulted in the lowest average error among the evaluated two-terminal methods. Thus, the generalizability of the proposed methodology for other power system structures and voltage levels is validated.

8. Conclusions

This paper presented a performance analysis of ten traditional impedance-based fault location methods, six based on one-terminal measurements and four based on two-terminal measurements, for lines connecting IBRs to the grid.

Boxplots were used to assess the percentage errors, evaluating their performance for a wide diversity of scenarios. With this, it was possible to notice the significant impact of IBRs on the performance of conventional impedance-based fault location methods.

The study enabled the proposition of a multi-method fault location methodology (Fig. 14) that, as was proven in this paper, significantly minimized the fault location errors on lines interconnecting IBRs, and can be a promising methodology, especially for conditions in which the communication channels between the line terminals are unavailable.

CRediT authorship contribution statement

Moisés J.B.B. Davi: Manuscript writing, System modeling in PSCAD, Conducting quantitative analyses, PSCAD simulations, Modeling the conventional fault location functions, Fault location methodology proposition, Results analysis, Manuscript revision. **Mário Oleskovicz:** Modeling the conventional fault location functions, Fault location methodology proposition, Results analysis, Manuscript revision. **Felipe V. Lopes:** Modeling the conventional fault location functions, Fault location methodology proposition, Results analysis, Manuscript revision.

Declaration of competing interest

The authors declare that they have no known competing financial interests or personal relationships that could have appeared to influence the work reported in this paper.

Data availability

Data will be made available on request.

Acknowledgments

This work was supported by the Sao Paulo Research Foundation (FAPESP), Brazil [grant #2022/00483-0] and the National Council for Scientific and Technological Development (CNPq), Brazil.

References

[1] Jones K, et al. Impact of inverter based generation on bulk power system dynamics and short-circuit performance. IEEE Power Energy Soc Tech Rep 2018.

[2] Davi MJBB, Jorge DC, Lopes FVa. Fault current and fault voltage analysis of power transmission systems with high penetration of inverter-based wind generators. Acta Sci Tech 2022;44. http://dx.doi.org/10.4025/actascitechnol.v44i1.57848.

[3] Kasztenny B. Line distance protection near unconventional energy sources. In: 16th international conference on developments in power system protection (DPSP 2022). 2022, p. 224–9. http://dx.doi.org/10.1049/icp.2022.0944.

[4] Davi MJBB, Oleskovicz M, Lopes FV, Jorge DC. A case study-based review of the impacts of inverter-interfaced wind power plants on distance protections. J Control Autom Electr Syst 2023;34:599–608. http://dx.doi.org/10.1007/s40313-023-00989-4.

[5] Haddadi A, Zhao M, Kocar I, Farantatos E, Martinez F. Impact of inverter-based resources on memory-polarized distance and directional protective relay elements. 2021, p. 1–6. http://dx.doi.org/10.1109/NAPS50074.2021.9449791.

[6] Davi MJBB, Oleskovicz M, Lopes FV, Jorge DC. Impacts of inverter-interfaced wind power plants in the phase-selection and directional protection functions. IEEE Lat Am Trans 2022;21:151–7. http://dx.doi.org/10.1109/TLA.2023.10015137.

[7] Hooshyar A, Iravani R. A new directional element for microgrid protection. IEEE Trans Smart Grid 2018;9(6):6862–76. http://dx.doi.org/10.1109/TSG.2017.2727400.

[8] Hooshyar A, El-Saadany EF, Sanaye-Pasand M. Fault type classification in microgrids including photovoltaic DGs. IEEE Trans Smart Grid 2016;7(5):2218–29. http://dx.doi.org/10.1109/TSG.2015.2451675.

[9] Banaiemoqadam A, Hooshyar A, Azzouz MA. A control-based solution for distance protection of lines connected to converter-interfaced sources during asymmetrical faults. IEEE Trans Power Deliv 2020;35(3):1455–66. http://dx.doi.org/10.1109/TPWRD.2019.2946757.

[10] IEEE. IEEE standard for interconnection and interoperability of inverter-based resources (IBRs) interconnecting with associated transmission electric power systems. IEEE Std 2800-2022 2022;1–180. http://dx.doi.org/10.1109/IEEESTD.2022.9762253.

[11] Das S, Santoso S, Gaikwad A, Patel M. Impedance-based fault location in transmission networks: theory and application. IEEE Access 2014;2:537–57. http://dx.doi.org/10.1109/ACCESS.2014.2323353.

[12] Ziegler G. Numerical distance protection: Principles and applications, 4th ed.. Germany, Erlangen: Publicis Publishing; 2011.

[13] Çapar A, Basa Arsoy A. Evaluating accuracy of fault location algorithms based on terminal current and voltage data. Int J Electr Electr Eng 2014;3. http://dx.doi.org/10.12720/ijeee.3.3.202-206.

[14] Takagi T, Yamakoshi Y, Yamaura M, Kondow R, Matsushima T. Development of a new type fault locator using the one-terminal voltage and current data. IEEE Trans Power Appar Syst 1982;PAS-101(8):2892–8. http://dx.doi.org/10.1109/TPAS.1982.317615.

[15] SEL. Advanced line differential protection, automation, and control system. 2018,

[16] Girgis A, Hart D, Peterson W. A new fault location technique for two- and three-terminal lines. IEEE Trans Power Deliv 1992;7(1):98–107. http://dx.doi.org/10.1109/61.108895.

[17] Johns AT, Jamali S. Accurate fault location technique for power transmission lines. IEEE Proc 1990;137(6):395–402. http://dx.doi.org/10.1049/ip-c.1990.0054.

[18] Preston G, Radojevic ZM, Kim CH, Terzija V. New settings-free fault location algorithm based on synchronised sampling. IEEE Proc 2011;5(3):376–83. http://dx.doi.org/10.1049/iet-gtd.2010.0053.

[19] He Z, Mai R, He W, Qian Q. Phasor-measurement-unit-based transmission line fault location estimator under dynamic conditions. GTD IET 2011;5:1183–91. http://dx.doi.org/10.1049/iet-gtd.2011.0081.

[20] Matthews RC, Hossain-McKenzie S, Reno MJ. Fault current correction strategies for effective fault location in inverter-based systems. In: 2019 IEEE 46th photovoltaic specialists conference. PVSC, 2019, p. 3124–31. http://dx.doi.org/10.1109/PVSC40753.2019.8980536.

[21] Chang F, Sun H, Kawano S, Nikovski D, Kitamura S, Su W. A fault detection and location technique for inverter-dominated islanding microgrids. In: 2022 IEEE 5th international electrical and energy conference. CIEEC, 2022, p. 2041–6. http://dx.doi.org/10.1109/CIEEC54735.2022.9846567.

[22] Panahi H, Sanaye-Pasand M, Davarpanah M. Three-terminal lines fault location using two main terminals data in the presence of renewable energy sources. IEEE Trans Smart Grid 2023;14(3):2085–95. http://dx.doi.org/10.1109/TSG.2022.3216908.

[23] Likhitha K, Naidu OD. Setting free fault location for three-terminal hybrid transmission lines connected with conventional and renewable resources. IEEE Access 2023;11:23839–56. http://dx.doi.org/10.1109/ACCESS.2023.3253506.

[24] Hooshyar A, Azzouz MA, El-Saadany EF. Distance protection of lines emanating from full-scale converter-interfaced renewable energy power plants—Part II: Solution description and evaluation. IEEE Trans Power Deliv 2015;30(4):1781–91. http://dx.doi.org/10.1109/TPWRD.2014.2369480.

[25] Lopes F, et al. Single-ended multi-method phasor-based approach for optimized fault location on transmission lines. Electr Power Syst Res 2022;212:108361. http://dx.doi.org/10.1016/j.epsr.2022.108361.

[26] Kauffmann T, et al. Short-circuit model for type-IV wind turbine generators with decoupled sequence control. IEEE Trans Power Deliv 2019;34(5):1998–2007. http://dx.doi.org/10.1109/TPWRD.2019.2908686.

[27] Tremblay O, Gagnon R, Fecteau M. Real-time simulation of a fully detailed type-IV wind turbine. In: International conference on power systems transients (IPST 2013). 2013.

[28] Miller N, Sanchez-Gasca J, Price W, Delmerico R. Dynamic modeling of GE 1.5 and 3.6 MW wind turbine-generators for stability simulations. In: 2003 IEEE power engineering society general meeting. vol. 3, 2003, p. 1977–83. http://dx.doi.org/10.1109/PES.2003.1267470.

[29] Commission UFER. Interconnection for wind energy docket no. RM05-4-001. 2005.

[30] Terzija VV, Dobrijevic DM. Short circuit studies in transmission networks using improved fault model. In: 2007 IEEE lausanne power tech. 2007, p. 1752–7. http://dx.doi.org/10.1109/PCT.2007.4538581.

[31] Andrade VD, Sorrentino E. Typical expected values of the fault resistance in power systems. In: 2010 IEEE/PES transmission and distribution conference and exposition: Latin America (T&D-la). 2010, p. 602–9. http://dx.doi.org/10.1109/TDC-LA.2010.5762944.